Effects of thickness & shape on localized surface plasmon resonance of sexfoil nanoparticles*

Yan Chen(陈艳)[1], Xianchao Liu(刘贤超)[1,2], Weidong Chen(陈卫东)[1], Zhengwei Xie(谢征微)[1], Yuerong Huang(黄跃容)[1], and Ling Li(李玲)[1,†]

[1] College of Physics and Electronic Engineering, Sichuan Normal University, Chengdu 610101, China
[2] State Key Laboratory of Electronic Thin Films and Integrated Devices, School of Optoelectronic Information, University of Electronic Science and Technology, Chengdu 610054, China

(Received 12 August 2016; revised manuscript received 23 September 2016; published online 30 November 2016)

Localized surface plasmon (LSPR) resonance and sensing properties of a novel nanostructure (sexfoil nanoparticle) are studied using the finite-difference time-domain method. For the sandwich sexfoil nanoparticle, the calculated extinction spectrum shows that with the thickness of the dielectric layer increasing, long-wavelength peaks blueshift, while short-wavelength peaks redshift. Strong near-field coupling of the upper and lower metal layers leads to electric and magnetic field resonances; as the thickness increases, the electric field resonance gradually increases, while the magnetic field resonance decreases. The obtained refractive index sensitivity and figure of merit are 332 nm/RIU and 3.91 RIU^{-1}, respectively. In order to obtain better sensing ability, we further research the LSPR character of monolayer Ag sexfoil nanoparticle. After a series of trials to optimize the thickness and shape, the refractive index sensitivity approximates 668 nm/RIU, and the greatest figure of merit value comes to 14.8 RIU^{-1}.

Keywords: sexfoil nanoparticle, localized surface plasmon resonance, extinction properties, LSPR sensors

PACS: 78.68.+m, 42.62.Be, 73.20.Mf, 78.67.−n **DOI:** 10.1088/1674-1056/26/1/017807

1. Introduction

The localized surface plasmon resonance (LSPR) is coherent oscillation of the free electron within a noble metal nanoparticle.[1,2] It is related to the size, material, shape, and surrounding dielectric environment of the metal nanoparticle.[3–6] When a noble metal nanoparticle is illuminated with an incident light, the electromagnetic energy is enhanced and highly localized near the metal-dielectric interface because of the interaction between the electromagnetic radiation and the nanoparticle.[7] This high intensity electric field (E-field) on the surface of the metal nanoparticle can be applied in surface-enhanced Raman scattering (SERS).[8–10] And because of their plasmonic properties, the noble metal nanoparticles can be used as components in a diverse range of technologies such as waveguides,[11] molecular rulers,[12] and photonic circuits.[13] Moreover, the LSPR spectrum of a nanoparticle is sensitive to the dielectric constant of the surrounding environment and is widely used in chemical/biological sensors.[14–17] In biochemical sensing applications, the sensing performance of metal nanoparticles is denoted with the figure of merit (FOM), which is defined as the shift of resonance wavelength per refractive index unit (RIU) divided by the line-width of the LSPR resonance peak.[18,19] To obtain a perfect FOM, the position of the resonance wavelength shift must be as long as possible or the line-width as narrow as possible.

Over the past few decades, many researchers have reported the optical properties and sensing performance of noble metal nanoparticles with various shapes, which are fabricated by different synthesis and nano fabrication methods.[20–23] In 2012, the gold nanorings were fabricated by Huang *et al.* by nanospherical-lens lithography (NLL). A biosensor based on nanorings showed a refractive index sensitivity (RIS, which is defined as the shift of resonance wavelength per refractive index unit) of 350 nm/RIU and a FOM of 3.1 RIU^{-1}.[24] In addition, Chang *et al.* successfully fabricated gold nanodisk arrays using the same method in 2013. The maximum FOM obtained in experiment was around 9 RIU^{-1}, and the RIS was about 300 nm/RIU.[25] In addition, some composite-structured nanoparticles with sharp angles, such as nano-stars,[26,27] nano-bowties,[28,29] and nano-crosses,[30] were studied in theory, and the results indicated that smaller vertex angles result in higher RIS and greater FOM. However, these nanoparticles are very difficult to realize in present experimental technology and conditions. In 2014, large-area, ordered sexfoil pore arrays were first fabricated on the surface of the photoresist using spherical-lens photolithography (SLP) by Geng *et al.*[31] On the bases of this nanopatterning, the sexfoil nanoparticle (SNP) can be easily produced by further experiments. It is worthwhile to further research this novel nanostructure experimentally and theoretically. Therefore, in this paper, we report our theoretical study of the sensing perfor-

*Project supported by the Sichuan Provincial Department of Education, China (Grant No. 16ZA0047), the State Key Laboratory of Metastable Materials Science and Technology, Yanshan University, China (Grant No. 201509), the Large Precision Instruments Open Project Foundation of Sichuan Normal University, China (Grant Nos. DJ201557, DJ201558 and DJ201560), and the State Key Laboratory of Optical Technologies on Nano Fabrication and Micro Engineering, Institute of Optics and Electronics, Chinese Academy of Sciences.

†Corresponding author. E-mail: lingli70@aliyun.com

© 2017 Chinese Physical Society and IOP Publishing Ltd

mance of a novel nanoparticle in detail.

For two closely-spaced SNPs, when the incident light is polarized along the center axes, the near field intensity is much stronger than that of an isolated nanoparticle due to coupling between them.[32–34] Adding a dielectric layer between two closely-spaced SNPs constitutes a novel sandwich sexfoil nanoparticle (SSNP). When tuning the resonance wavelength, it is more convenient and easier to change the dielectric layer thickness of this nanostructure than to change the geometric size and shape of the single layer nanostructure.[27] In the present study, the novel nanostructure (SSNP) consists of two metal (Ag) layers and a dielectric (MgF_2) layer. At first, an SSNP model is developed using the CST Microwave Studio software. The extinction spectra of SSNPs with various thicknesses of the dielectric layer are obtained by the finite-difference time-domain (FDTD) method. Based on the extinction spectra, the LSPR sensing properties with different environmental refractive indices are analyzed. In order to obtain better sensing properties, we also develop a monolayer Ag SNP and study the optical properties and sensing performance through adjusting its thickness and shape.

2. Simulation and modeling

The geometry of an Ag/MgF_2/Ag SSNP is defined by four parameters: the side length l of the central hexagon, the half of short axis a of the half ellipse, the thickness t of the intermediate dielectric layer, and the thickness h of the top and bottom silver layers. Figure 1 shows the x–y cross section and the three-dimensional (3D) plot of a single SSNP. The r, which is half of the width of the central hexagon, is defined as $r = l\cos 30°$. Each SNP has the same surface area of 13079 nm^2. All numerical calculations are performed on the basis of the FDTD method in the CST Microwave Studio software, which is popular and flexible for calculating optical properties of metal nanoparticles with arbitrary shape.

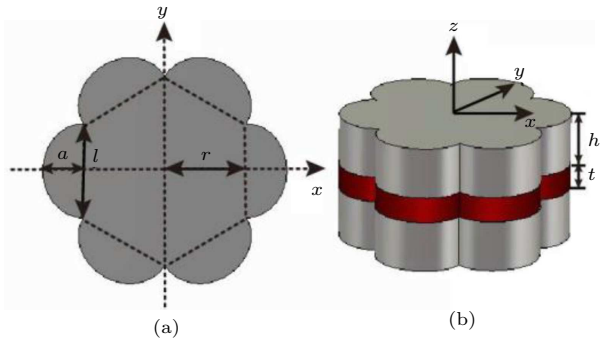


Fig. 1. (color online) Sketch of a single SSNP. (a) The x–y cross section of the nanoparticle is composed of a central hexagon and six semi-ellipses joined at its edges. (b) Three-dimensional shape of the SSNP.

In our calculations, the Ag/MgF_2/Ag SSNP is embedded in air, the complex relative dielectric constant of the silver is cited from Ref. [35], and the refractive index of MgF_2 is set to be 1.38 at 550 nm of light wavelength. Perfectly matched layer (PML) boundary conditions are imposed at the boundaries of the calculation domain, which is large enough to avoid interaction between two particles and truncation of the field. A discrete tetrahedral mesh with a spacing of 2.5 nm is used. The illumination light with TM polarization is normal to the surface of the SSNP along the negative z axis.

3. Results and discussion

The extinction efficiencies of the Ag/MgF_2/Ag SSNPs with different thicknesses of dielectric layer are investigated by the FDTD method. Here, the thicknesses of the upper and lower Ag layers are fixed at 20 nm. Figure 2(a) shows that the

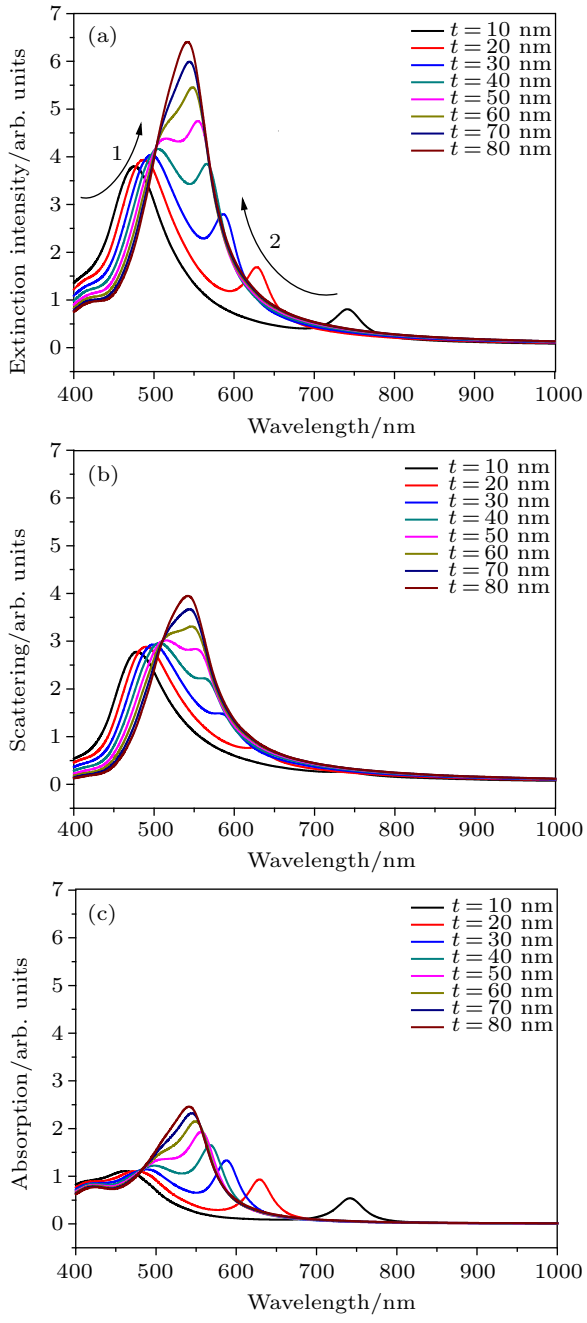


Fig. 2. (color online) (a) Extinction, (b) scattering, and (c) absorption spectra with changing thickness of the dielectric layer; the thicknesses of the top and bottom Ag layers are both 20 nm.

extinction spectra have two clear resonance peaks 1 and 2 located respectively at 475 nm and 745 nm when the thickness of the dielectric layer is 10 nm. As the thickness of the dielectric layer is increased from 10 nm to 80 nm, the extinction efficiency becomes higher, and peak 1 at short wavelength generates redshift, whereas blueshift is generated at the longer-wavelength peak 2. When the thickness is increased to 80 nm, the two resonance peaks are superposed into one peak located at 550 nm, and the extinction efficiency reaches its maximum value.

The extinction efficiency $\sigma_{\text{ext}}(\lambda)$[36,37] can be described as

$$\sigma_{\text{ext}}(\lambda) = \sigma_{\text{sca}}(\lambda) + \sigma_{\text{abs}}(\lambda). \quad (1)$$

Here, $\sigma_{\text{sca}}(\lambda)$ and $\sigma_{\text{abs}}(\lambda)$ are the scattering and absorption efficiencies of the nanoparticle, respectively. Figures 2(b) and 2(c) display the scattering and absorption spectra of the SSNPs with different thicknesses of the dielectric layer; the upper and lower silver layers are 20 nm. The short wavelength peak 1 emerges from the electric dipolar resonance, whereas peak 2 at longer wavelength comes from the magnetic dipolar resonance. Figure 2(b) shows redshift of the electric dipolar resonance with increasing thickness of the dielectric layer, while the magnetic dipolar resonance remains unchanged. However, as the thickness of the dielectric layer is increased, the magnetic dipolar resonance blueshifts and the electric dipolar resonance remains almost unchanged (Fig. 2(c)). A comparison of the resonance peak positions in extinction, scattering, and absorption spectra reveals that the redshift of peak 1 is closely related to the variation of the scattering efficiency, and the absorption efficiency affects the shift of peak 2.

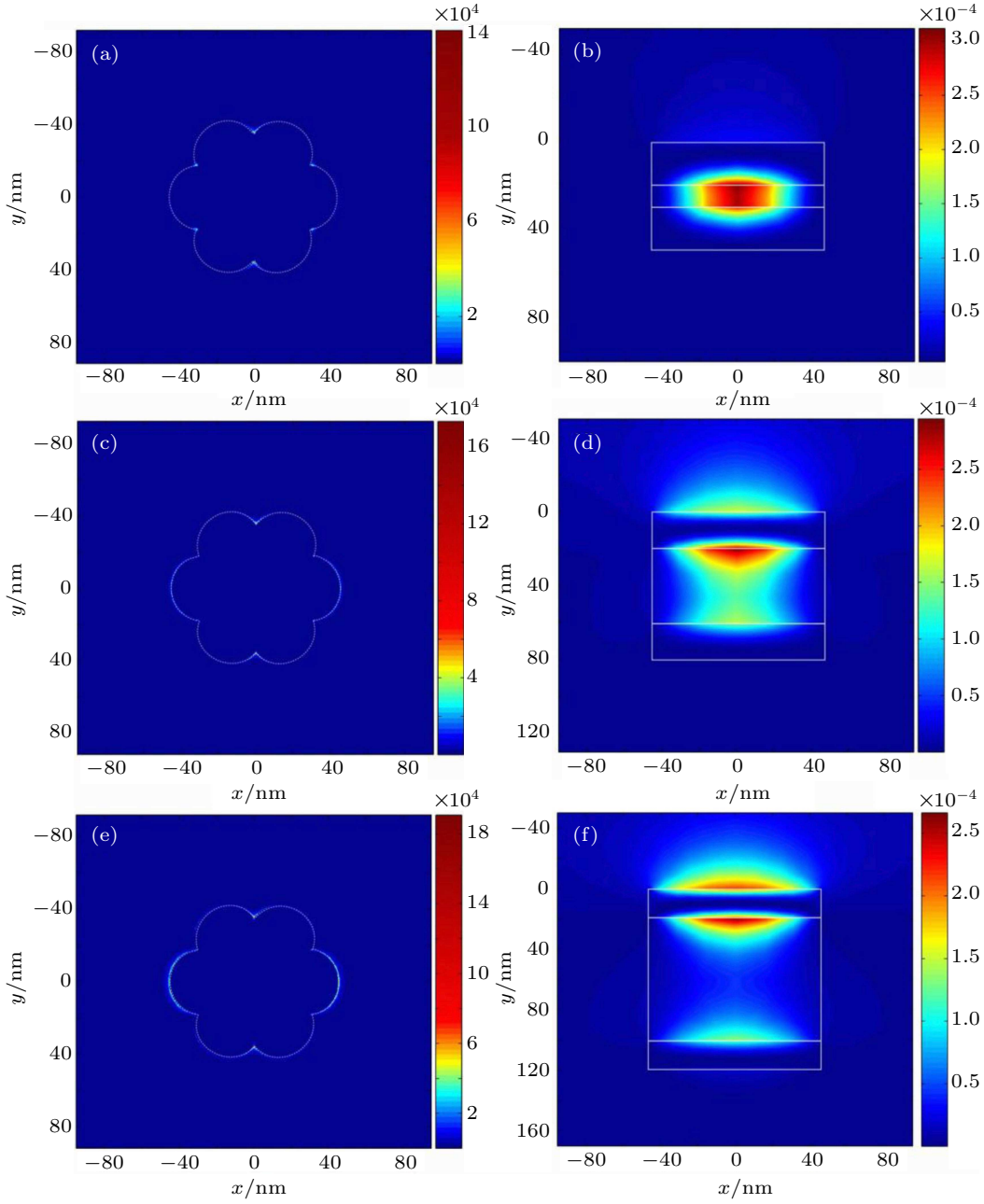


Fig. 3. (color online) Electric field distribution of x–y plane with different thicknesses of the MgF_2 layer: (a) $t = 10$ nm, (c) $t = 40$ nm, and (e) $t = 80$ nm. Magnetic field distribution of x–z plane with different thicknesses of the MgF_2 layer: (b) $t = 10$ nm, (d) $t = 40$ nm, and (f) $t = 80$ nm. The thicknesses of the top and bottom Ag layers are both 20 nm.

The spectral shifts of the SSNP can be explained by plasmon hybridization theory.[38–40] When the upper and lower metal layers interact, plasmon hybridization is excited and the initial degenerate plasmon mode splits into two resonances: symmetric resonance and antisymmetric resonance.[41,42] In the plane, the symmetric resonance, which has an electric dipolar character, is parallel to the surface of the SSNP. While the antisymmetric resonance with a dipolar magnetic moment is perpendicular to the surface plasmon direction.[43,44] As the dielectric layer is made thicker, the vertical plasmon coupling gradually reduces.[45] For the Ag/MgF_2/Ag SSNP with the thicknesses of the dielectric layer at 10 nm, 40 nm, and 80 nm, the intensity distributions of the electric and magnetic fields are displayed in Fig. 3. The E-field intensity of the nanoparticle is stronger with the thickness of the MgF_2 layer increasing, as revealed in Figs. 3(a), 3(c), and 3(e). With MgF_2 layer thickness increasing, the greater E-field enhancement and more effective concentration of E-field contribute to the redshift in resonance wavelength (short-wavelength peak in the scattering spectra). Figures 3(b), 3(d), and 3(f) indicate that as the MgF_2 layer thickness increases, the magnetic resonance and interaction between the upper and lower silver layers are both weakened gradually, which leads to the blueshift of the long-wavelength peak in the absorption spectra. When the thickness increases to 80 nm, both the short-wavelength peak and long-wavelength peak shift to the point where the wavelength is 550 nm. So only one resonance peak occurs due to the superposition of two resonance peaks in the LSPR spectra when $t = 80$ nm. In addition, the intensity of the LSPR spectra with a thicker dielectric layer is stronger than that for the thinner layer because of the superposition. In other words, the full-width at half-maximum (FWHM) of the LSPR spectra reduces with the thickness of the dielectric layer increasing from 10 nm to 80 nm. When $t = 80$ nm, the FWHM is 85 nm. In this case, the extinction spectra of different environmental refractive index are obtained, as shown in Fig. 4(a). When the refractive index varies from 1.0 to 1.5 in intervals of 0.1, substantial redshift of the extinction peak is observed. For example, when the refractive index increases from 1.0 to 1.1, the corresponding resonance wavelength slowly rises from 541.4 nm to 571.4 nm. Figure 4(b) shows that the sensing ability of the resonance wavelength to the environment refractive index can be estimated by linear fitting. The RIS of the Ag/MgF_2/Ag SSNP is 332 nm/RIU, with the linear correlation coefficient 0.99943. The FOM, which is defined as FOM = RIS/FWHM,[46,47] is about 3.91 RIU^{-1}.

Although adjusting the intermediate dielectric layer thickness of the SSNPs is easier than adjusting the geometric size of the monolayer SNPs, the obtained FWHM and FOM are not ideal. In order to obtain narrower FWHM and better FOM, we remove the intermediate dielectric layer, and further

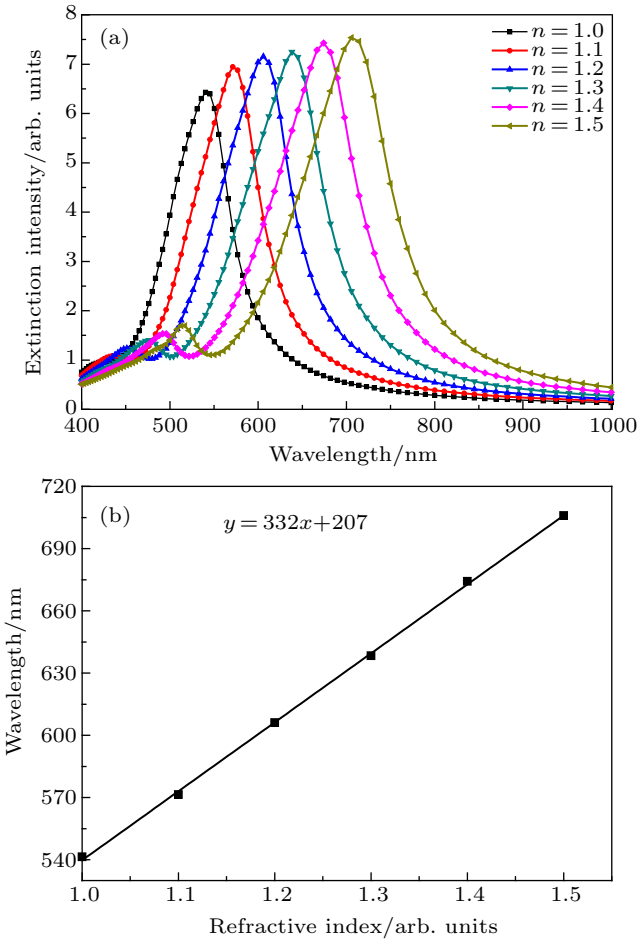


Fig. 4. (color online) (a) Extinction spectra in the surrounding media of different indexes for a single Ag/MgF_2/Ag SSNP. (b) Extinction peaks as a function of the refractive index. The solid line is a linear fit of the discrete positions.

investigate the extinction spectra and sensing performance of single layer Ag SNPs. In the simulation, all the SNPs have a same surface area as the SSNPs. Figure 5 displays the extinction efficiency of the monolayer Ag SNPs with thicknesses from 10 nm to 50 nm. It indicates that as the thickness increases, the resonance wavelength blueshifts. Table 1 shows that the FWHM decreases gradually with the Ag monolayer thickness reducing, while the RIS increases. When $h = 10$ nm, the RIS is 472 nm/RIU, and the FOM is 10.8 RIU^{-1}. Compared with a nanodisk of the same size, the E-field distribution near the sharp edges of the SNP is more localized and intensified. It contributes to the increase of the extinction efficiency and redshift of the resonance wavelength.[26] So the RIS of the SNP is higher than that of the nanodisk of the same size, contributing to the better FOM of the SNP.

Table 1. Widths of extinction spectra, calculated refractive index sensitivity, and figure of merit of the Ag SNPs with different thicknesses.

h/nm	10	20	30	40	50
FWHM/nm	44	51	56	64	71
RIS/nm·RIU^{-1}	473	396	374	352	340
FOM/RIU^{-1}	10.8	7.8	6.7	5.5	4.8

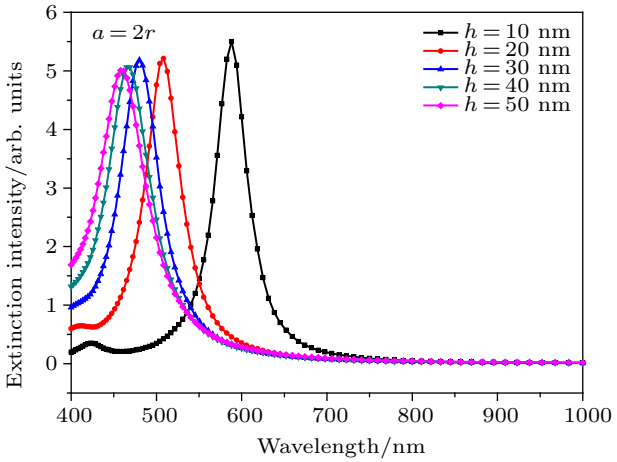


Fig. 5. (color online) LSPR spectra of single unilaminar Ag SNPs with different thicknesses.

When an SNP serves as an LSPR sensor, the sensing characteristics are also affected by its shape. Now, we consider the influence of the shape on its optical properties and sensing performance. In the simulation, the thickness of the silver layer is $h = 10$ nm, and the ratio a/r increases from 0.5 to 2.0. Figure 6 describes the extinction intensities of single monolayer Ag SNPs with four different ratios. It is readily apparent that the resonance wavelength redshifts with the ratio decreasing. In addition, the resonance peak width has almost no change. Calculation results indicate that the smaller ratio results in higher refractive index sensitivity (the maximum value reaches 668 nm/RIU), but the FWHM changes slightly (see Table 2). Moreover, the FOM increases gradually as the ratio reduces, and it reaches 14.8 RIU^{-1} when $a = 0.5r$.

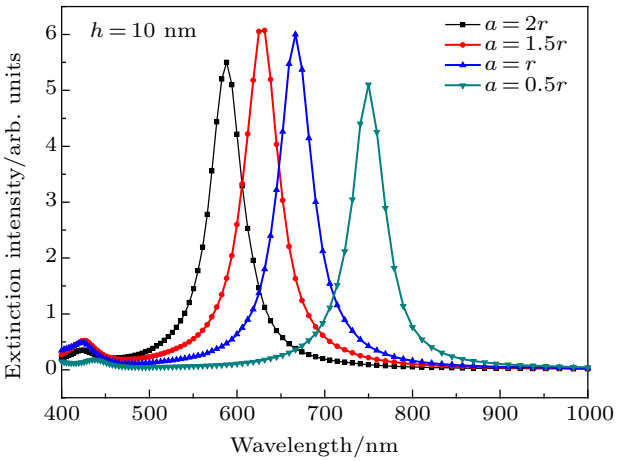


Fig. 6. (color online) Plasmon resonance spectra of four different ratios.

Table 2. Widths of extinction spectra, calculated refractive index sensitivity, and figure of merit for four different ratios.

a/r	2	1.5	1	0.5
FWHM/nm	44	48	47	45
RIS/nm·RIU^{-1}	473	528	570	668
FOM/RIU^{-1}	10.8	11	12.1	14.8

4. Conclusion

In summary, we have presented a novel nanostructure (SNP) and studied theoretically the localized surface plasmon (LSPR) resonance and sensing properties of different thicknesses and shapes. The calculated extinction spectra of SSNPs reveal that with the thickness of the dielectric layer increasing, long-wavelength peaks blueshift, while short-wavelength peaks redshift. The correlations, which link the maximum of the electromagnetic fields enhancement with the thickness of the dielectric layer, reveal that as the thickness increases, the electric field resonance gradually increases, while the magnetic field resonance decreases. This phenomenon is explained by the plasmon hybridization theory. For SSNPs serving as LSPR sensors, when the dielectric layer thickness t is 80 nm, the refractive index sensitivity and figure of merit are 332 nm/RIU and 3.91 RIU^{-1}, respectively. To obtain better sensing performance, we remove the intermediate dielectric layer and study the extinction efficiency of the single monolayer Ag SNPs with different thicknesses and ratios a/r. It is found that when either the thickness or ratio a/r is reduced, the refractive index sensitivity and figure of merit both strengthen gradually. Through a series of optimizing, we find that when the metal layer thickness h is 10 nm and $a = 0.5r$, the RIS comes to 668 nm/RIU and the FOM is 14.8 RIU^{-1}. These results can offer some valuable guidelines to the designers of SNP-based sensors.

References

[1] Hao J Y, Xu Y, Zhang Y P, Chen S F, Li X A, Wang L H and Huang W 2015 *Chin. Phys. B* **24** 045201
[2] Hutter E and Fendler J H 2004 *Adv. Mater.* **16** 1685
[3] Kelly K L, Coronado E, Zhao L L and Schatz G C 2003 *J. Phys. Chem. B* **107** 668
[4] Li T, Yu L, Lu Z X, Song G and Zhang K 2011 *Chin. Phys. B* **20** 087805
[5] Ye J and Van D P 2012 *Nanoscale* **4** 7205
[6] Liu Z Q, Shao H B, Liu G Q, Liu X S, Zhou H Q, Hu Y, Zhang X N, Cai Z J and Gu G 2014 *Appl. Phys. Lett.* **104** 081116
[7] Peng L, Mei Y, Chen S F, Zhang Y P, Hao J Y, Deng L L and Huang W 2015 *Chin. Phys. B* **24** 115202
[8] Ci X T, Wu B T, Song M, Chen G X, Liu Y, Wu E and Zeng H P 2014 *Chin. Phys. B* **23** 097303
[9] Wang B B, Zhou J, Zhang H P and Chen J P 2014 *Chin. Phys. B* **23** 087303
[10] Jiang S M, Wu D J, Cheng Y and Liu X J 2012 *Chin. Phys. B* **21** 127806
[11] Maier S A, Kik P G, Atwater H A, Meltzer S, Harel E, Koel B E and Requicha A A G 2003 *Nat. Mater.* **2** 229
[12] Chowdhury M H, Ray K, Gray S K, Pond J and Lakowicz J R 2009 *Anal. Chem.* **81** 1397
[13] Zhou X, Fu Y, Li K, Wang S and Cai Z 2008 *Appl. Phys. B* **91** 373
[14] Wang B B, Zhou J, Chen D, Fang Y T and Chen M Y 2015 *Chin. Phys. B* **24** 087301
[15] Anker J N, Hall W P, Lyandres O, Lyandres O, Shah N C, Zhao J and Duyne R P V 2008 *Nat. Mater.* **7** 442
[16] Hotta K, Yamaguchi A and Teramae N 2012 *ACS Nano* **6** 1541
[17] Chen L, Wei H, Chen K Q and Xu H X 2014 *Chin. Phys. B* **23** 027303
[18] Dong P P, Wu Y T, Guo W Y and Di J W 2013 *Plasmonics* **8** 1577
[19] Piliarik M, Kvasnika P, Galler N, Krenn J R and Homola J 2011 *Opt. Express* **19** 9213
[20] Augui B and Barnes W L 2009 *Opt. Lett.* **34** 401
[21] Husu H, Mkitalo J, Laukkanen J, Kuittinen M and Kauranen M 2010 *Opt. Express* **18** 16601

[22] Liu J, Chen Y S, Cai H Y, Chen X Y, Li C W and Yang C F 2015 *Material* **8** 2688
[23] Sekhon J S and Verma S S 2015 *J. Mod. Optic.* **62** 435
[24] Huang C, Ye J, Wang S, Stakenborg T and Lagae L 2012 *Appl. Phys. Lett.* **100** 173114
[25] Chang Y C, Chung H C, Lu S C and Guo T F 2013 *Nanotechnology* **24** 095302
[26] Ma W Y, Yang H, Hilton J P, Lin Q, Liu J Y, Huang L X and Yao J 2010 *Opt. Express* **18** 843
[27] Luo J, Qiu C K, Wang W M and Lin Q 2014 *Appl. Opt.* **53** 3528
[28] Bi G, Wang L, Ling L, Yokota Y, Nishijima Y, Ueno K, Misawa H and Qiu J 2013 *Opt. Commun.* **294** 213
[29] Wang Q, Wu S F, Li X F and Wang X G 2010 *Chin. Phys. B* **19** 117304
[30] Zhang M J, Zhou X L and Fu Y Q 2010 *Plasmonics* **5** 355
[31] Geng C, Yan Q F, Du C X, Dong P, Zhang L J, Wei T B, Hao Z B, Wang X Q and Shen D Z 2014 *ACS Photonics* **sl1** 754
[32] Su K H, Wei Q H Zhang X, Mock J J, Smith D R and Schultz S 2003 *Nano Lett.* **3** 1087
[33] Atay T, Song J H and Nurmikko A V 2004 *Nano Lett.* **4** 1627
[34] Dahmen C, Schmidt B and Plessen G 2007 *Nano Lett.* **7** 318
[35] Palik E D 1998 *Handbook of Optical Constants of Solids* (New York: Academic Press)
[36] Yang L Y, Du C L and Luo X G 2009 *J. Nanosci. Nanotechno.* **9** 2660
[37] Hong Y, Huh Y M, Yoon D S and Yang J 2012 *J. Nanomater.* 111
[38] Fischer J, Vogel N, Mohammadi R, Butt H, Landfester K, Weiss C K and Kreiter M 2011 *Nanoscale* **3** 4788
[39] Koya A N, Ji B, Hao Z, Hao Z Q and Lin J Q 2015 *J. Appl. Phys.* **118** 113101
[40] Nordlander P, Oubre C and Prodan E 2004 *Nano Lett.* **4** 899
[41] Li X, Yang L Y, Hu C G, Luo X G and Hong M H 2011 *Opt. Express* **19** 5283
[42] Liu N, Guo H C, Fu L W, Kaiser S, Schweizer H and Giessen H 2007 *Adv. Mater.* **19** 3628
[43] Evanoff D D and Chumanov G 2005 *Chem. Phys. Chem.* **6** 1221
[44] Ekinci Y, Christ A, Agio M, Martin O J F, Solak H H and Lffler J F 2008 *Opt. Express* **16** 13287
[45] Pakizeh T, Abrishamian M S Granpayeh N, Dmitriev A and Kll M 2006 *Opt. Express* **14** 8240
[46] Špačková B and Homola J 2013 *Opt. Express* **21** 27490
[47] Navas M P and Soni R K 2014 *Appl. Phys. A* **116** 879